



Residual Stresses from Incremental Hole Drilling Using Directly Deposited Thin Film Strain Gauges

S. Heikebrügge¹ · R. Ottermann² · B. Breidenstein¹ · M.C. Wurz² · F. Dencker²

Received: 6 September 2021 / Accepted: 6 January 2022 / Published online: 14 January 2022
© The Author(s) 2022

Abstract

Background Commonly, polymer foil-based strain gauges are used for the incremental hole drilling method to obtain residual stress depth profiles. These polymer foil-based strain gauges are prone to errors due to application by glue. For example zero depth setting is thus often erroneous due to necessary removal of polymer foil and glue. This is resulting in wrong use of the calibration coefficients and depth resolution and thus leading to wrong calculations of the obtained residual stress depth profiles. Additionally common polymer foil-based sensors are limited in their application regarding e.g. exposure to high temperatures.

Objective This paper aims at a first step into the qualification of directly deposited thin film strain gauges for use with the incremental hole drilling method. With the directly deposited sensors, uncertainties regarding the determination of calibration coefficients and zero depth setting due to the absence of glue can be reduced to a minimum. Additionally, new areas of interest such as the investigation of thermally sprayed metallic layers can be addressed by the sensors due to their higher temperature resilience and their component inherent minimal thickness.

Methods For the first time, different layouts of directly deposited thin film strain gauges for residual stress measurements were manufactured on a stainless steel specimen. Strain measurements during incremental hole drilling using a bespoke hole drilling device were conducted. Residual stress depth profiles were calculated using the Integral method of the ASTM E837 standard. Afterwards, strain measurements with conventional polymer foil-based strain gauges during incremental hole drilling were conducted and residual stress depth profiles were calculated accordingly. Finally the obtained profiles were compared regarding characteristic values.

Results The residual stress depth profiles obtained from directly deposited strain gauges generally match the ones obtained from conventional polymer foil based strain gauges. With the novel strain gauges, zero depth setting is simplified due to the absence of glue and polymer foil. With the direct deposition, a wide variety of rosette designs is possible, enabling a more detailed evaluation of the strain field around the drilled hole.

Conclusions The comparative analysis of the obtained residual stress depth profiles shows the general feasibility of directly deposited strain gauges for residual stress measurements. Detailed investigations on uncertainty sources are still necessary.

Keywords Thin-film strain gauges · Incremental hole-drilling method · Residual stress · Direct deposition · Temperature sensors · Sputtering

✉ S. Heikebrügge
heikebruegge@ifw.uni-hannover.de

R. Ottermann
ottermann@impt.uni-hannover.de

B. Breidenstein
breidenstein@ifw.uni-hannover.de

M.C. Wurz
wurz@impt.uni-hannover.de

F. Dencker
dencker@impt.uni-hannover.de

¹ Institute of Production Engineering and Machine Tools, Leibniz University Hannover, An der Universität 2, 30823 Garbsen, Germany

² Institute of Micro Production Technology, Leibniz University Hannover, An der Universität 2, 30823 Garbsen, Germany



Introduction

The incremental hole drilling method is widely used for residual stress measurements of metallic, ceramic or polymer components. It can be used to quantify the residual stress state generated by manufacturing processes or e.g. to quantify the residual stress state of components that were already in use for a certain amount of their service life. Residual stress depth profiles are calculated based on relieved strains during high speed drilling, where a small hole with a diameter of approx. 2 mm and a depth of approx. 1 mm is created gradually. The removal of material leads to a stress relaxation and therefore also a strain relaxation. These relaxed strains are detected by strain gauges that are located around the measuring spot in the form of a rosette. Conventionally, polymer foil-based strain gauges are glued onto the mostly metallic components. This paper shows a new approach for the detection of strains during high speed drilling, which is the direct deposition of thin-film strain gauges. The sensor is directly applied on the component itself, without the need for an adhesive. This leads to lower sensor thickness below 3 μm and therefore measurements which are as close to the surface as possible, resulting in higher adhesion properties and prevention of possible measurement errors that can occur because of the adhesive or the application process by the user of conventional strain gauges. Thus, perforating of polymer-film and glue during zero-point setting can be omitted. Due to the polymer-free sensor system, a higher temperature resilience up to at least 400 $^{\circ}\text{C}$ compared to polymer foil-based is given [1]. In combination with the minimal sensor thickness, new areas of interest can be addressed by directly deposited sensors. One example is the investigation of thermally sprayed metallic layers. Conventionally, the strain gauges for the incremental hole drilling method in this context are attached on top of the thermally sprayed metal coating after its application [2], as shown in Fig. 1 (green). This is making it necessary to adapt calculation methods, because of different material states throughout the thick film system. Currently the adaptations are only approximations, also because of possible high interface roughness [3, 4]. Directly deposited sensors (red) enable the deposition prior to the thermal spray process. Therefore, completely new positions are enabled which have the potential to generate new information about the stress state at the interface between thermally sprayed coating and substrate. In general, an improvement of the characterisation of various layer compounds with the incremental hole drilling method is expected, enabled by the usage of directly deposited sensors, which has not been used in the literature before.

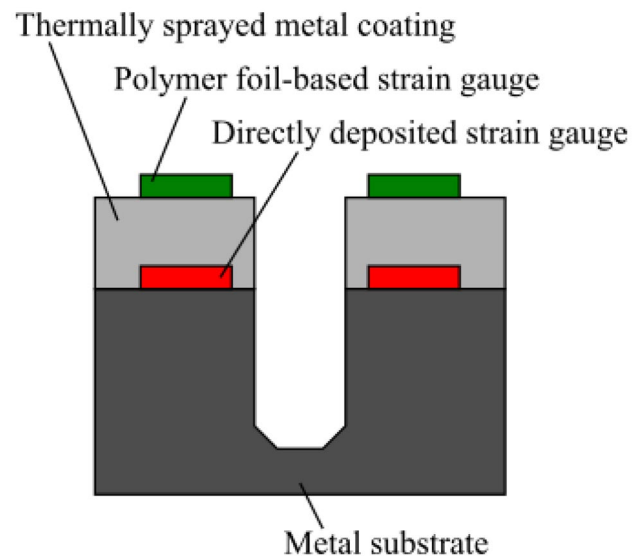


Fig. 1 Exemplary application of directly deposited strain gauges

State of the Art

Incremental Hole Drilling

The incremental hole drilling method using strain gauges has been widely used in the past. The first investigations of the test method began in the 1960s by Rendler and Vigness [5], leading to a standardization of the test method itself using standardized strain gauges and standardized calculation steps [6]. Following the works of Schajer [7, 8], the integral method was found to be the most practical method for the calculation of non-uniform residual stresses. Thus, this method is recorded inside the ASTM E837 standard [6]. The integral method needs calibration coefficients to convert the strains measured on the surface of a component into depth resolved subsurface residual stresses. These calibration coefficients are necessarily derived by Finite Element simulations. Most of the studies found in literature investigate the influence of cutter or hole geometry [9, 10], material properties [11] or specimen geometry [12] on the calibration coefficients. In any study considered, the relieved strains are evaluated directly on the surface of the Finite Element mesh. Technically, these studies do not consider that in conventional incremental hole drilling the relieved strains are recorded by polymer foil embedded metal based filaments. Additionally, the studies do not consider that the strain gauge rosettes are glued onto the measuring object. This results in a neglect of possible varying thicknesses of the adhesive and differences in mechanical and thermal properties of substrate, adhesive and polymer foil.



Uncertainties In Incremental Hole Drilling Regarding Strain Measurements And Zero Depth Setting

Several studies investigated measurement uncertainties and errors of the incremental hole drilling method [13–16]. Most influential error sources regarding strain measurements are:

1. Instrumentation errors
2. Measurement device errors
3. Measurement of apparent strains due to heat input generated by drilling

None of the studies mentioned above quantify the errors induced by instrumentation, whereby the quality of the strain gauge application significantly depends on the user. Differences in specimen preparation and adhesive thickness have to be considered. It is evident that differences in surface preparation and adhesive application significantly influence the transmission of strains from the surface of the component to the metal filament inside the polymer film [17].

In conventional incremental hole drilling, zero depth setting is comparably prone to errors. This is due to the fact that the polymer film of the strain gauge rosette and the adhesive have to be removed completely by initial drilling steps [6]. In these drilling steps it is possible that the drill is clogged with the polymer materials, often resulting in getting stuck. During the removal of polymer foil and adhesive it is also possible that surface near material of the specimen is already removed, resulting in a zero depth offset. This in fact influences the residual stress calculation procedure, because the above mentioned calibration coefficients are derived for exact distances to the surface or zero depths. A correction for the zero depth offset is possible, yet often not conducted due to difficulties in measurement of the offset [14, 15].

Strain and Temperature Measurements Using Directly Deposited Thin Film Strain Gauges

Conventional resistive foil-based strain gauges consist of a polyimide substrate resulting in total thicknesses of 40–80 μm [18]. As already mentioned, due to the substrate foil and the adhesive for application, measurement errors can occur [19, 20]. Long-time measurements and elevated temperature can reveal a creeping phenomenon resulting in relative uncertainties after a measurement duration of 20 h of 1% at 23 $^{\circ}\text{C}$ or 9% at 160 $^{\circ}\text{C}$ [21]. The maximum short term operation temperature of common strain gauges is 350 $^{\circ}\text{C}$ [21]. Directly deposited thin-film strain gauges with thicknesses of below 5 μm can overcome these disadvantages [22, 23]. The sensors are directly manufactured on the surface of the component [24, 25]. For metallic technical surfaces,

an insulation layer is necessary before the sensor layer is applied and structured by shadow masks, photolithography or laser ablation. Depending on the application, a top coat is applied in the end. For this whole manufacturing process, the Institute of Micro Production Technology of the Leibniz University Hannover developed a patented coating system [26–28]. Manufactured strain gauge sensors were able to withstand maximum operation temperatures up to 400 $^{\circ}\text{C}$ and showed higher temperature compensation capability compared to common sensors [1, 29]. Thin-film-based sensors have been integrated into metal tools to measure process parameters in industrial processes such as sheet temperature during mold hardening or material flow of the metal sheet during deep drawing [30, 31].

Through special design of a wear protection layer and an insulation layer, it was possible to guarantee the functionality of the sensors even at temperatures in the range of over 500 $^{\circ}\text{C}$ and at the same time considerable surface pressures over 1.5 GPa [32]. Even strain measurements on curved metallic surfaces are possible [33].

The state of the art shows that it is possible to measure strains by directly depositing strain gauges onto the surface of components. A use of directly deposited sensors for residual stress measurements by incremental hole drilling would overcome the neglects made in derivation of calibration coefficients. Additionally it would minimize the above mentioned errors or uncertainties in strain measurement and zero depth setting. Thus, the following study investigates the feasibility of the incremental hole drilling method using directly deposited thin film strain gauges.

Experimental Setup

Sensor Design

For the authors knowledge, directly-deposited strain gauges have not been used for the incremental hole-drilling method so far. In order to use the existing methods of sensor data analysis, the photo masks which are necessary for the thin-film sensor manufacturing, are designed based on CEA-06-062UL-120 and CEA-06-062UM-120 from Vishay Precision Group Inc. (Fig. 2, [34]). Especially parameters as the drilling hole diameter between 1.5 mm and 2.0 mm, the measurement grid centre diameter of 5.13 mm and the sensor length of 1.57 mm per strain gauge remain the same.

Sensor Manufacturing

The investigations take place on a plane stainless-steel sample (AISI 304) with dimensions of 100 mm \times 100 mm \times 6 mm. Any residual stresses measured originate from manufacturing of the sheet, followed by surface preparation (e.g. grinding



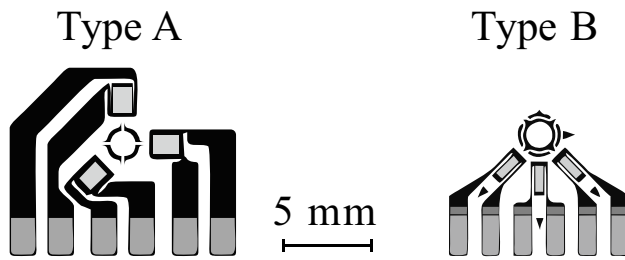


Fig. 2 Hole drilling rosette types [6, 34]

and polishing). The sample material is a classic representative for stainless steel objects with lots of thin film technology experience. A summary of the most important properties of this steel is given in Table 1. The usage of other substrate materials (different metals, ceramics, glass) is possible as well. There are only a few limitations that can occur due to porosity or roughness, e.g. when polishing cannot take place. Curved surfaces are possible as well, as [33] showed. The material has to be suitable for vacuum regarding the deposition process to manufacture the sensors. Consequently, the deposition on synthetic materials is a challenge, whereas for example the usage of polyether ether ketone (PEEK) is possible.

First, grinding and polishing reduce the arithmetic mean roughness R_a from $0.158 \pm 0.007 \mu\text{m}$ to $0.014 \pm 0.005 \mu\text{m}$ and the mean roughness depth R_z from $1.375 \pm 0.171 \mu\text{m}$ to $0.181 \pm 0.047 \mu\text{m}$. This is necessary to enable the production of an insulation layer of high insulation quality. Therefore, the surface roughness tester type HOMMEL-ETAMIC W5 from JENOPTIK was used. The measurement length was 4.8 mm, the velocity 0.5 mm/s and a filter according to ISO 11562 was applied [36]. Of course, the used surface preparation can lead to shallow residual

stresses that would influence the results from the measurements conducted. According to [37] this influence occurs but vanishes exponentially with depth after 30 μm . Therefore, it is neglected in this study. Moreover the comparison of directly deposited sensors and foil-based sensors (attached without additional grinding) took place on the same specimen with same surface preparation, which enables a comparison of the measurement results. After a cleaning step with acetone and isopropanol in an ultrasonic bath for 5 min each, a Kenotec MRC RF magnetron sputter coating system is used for all following thin-film depositions that always start with a sputter etching process at 250 W with 50 sccm Argon for 2 min resulting in a process pressure of $9.3 \cdot 10^{-4}$ mbar.

With a base pressure of $8 \cdot 10^{-8}$ mbar and a sputtering pressure of $6.7 \cdot 10^{-3}$ mbar, an alumina (Al_2O_3) insulation layer with a thickness of 2 μm is applied. The mass flows of Argon and Oxygen are 95 sccm and 5 sccm. This generates layers with optimized stoichiometry. This reactive sputtering process with a power density of 214 W/cm^2 is conducted in two steps of 3 h each with another cleaning step in between and afterwards to minimize the formation of pin-holes and to remove particles which would both lead to inadequate insulation properties. Alumina is used due to its high insulation properties, high adhesion on steel and its thermal expansion coefficient of about 8.5 $\text{ppm}/^\circ\text{C}$ [38] which is quite close to the coefficient of 16 $\text{ppm}/^\circ\text{C}$ [35] for stainless-steel compared to other common insulation materials like SiO_2 (0.5 $\text{ppm}/^\circ\text{C}$) or Si_3N_4 (1.4 $\text{ppm}/^\circ\text{C}$).

Then, the strain gauge sensor layer of Nickel–Chromium 60/40 (NiCr) with a thickness of 130 nm is deposited and structured with a lift-off process. Therefore, an AZ@ 5214 E image reversal resist from MicroChemicals is used in positive mode. After spin-coating at 1,000 rpm and a

Table 1 Properties of stainless steel type AISI 304 [35]

Property	Unit		Value				
Density	kg/dm ³		7.9				
Electrical resistivity	$\Omega\text{mm}^2/\text{m}$		0.73				
Thermal conductivity	W/(mK)		15				
Specific heat capacity	J/(kgK)		500				
Thermal expansion	ppm/ $^\circ\text{C}$		16				
Yield strength $R_{p0.2}$	N/mm ²		≥ 190				
Tensile strength R_m	N/mm ²		500–700				
Tensile elongation A_5	%		≥ 45				
Hardness (HB)	-		≤ 215				
Element	C	Cr	Ni	Mn	Si	N	S
wt% Min	-	17.5	8.0	-	-	-	-
wt% Max	0.07	19.5	10.5	2.0	1.0	0.1	0.03



softbake at 105 °C for 100 s, a mask aligner MA6 from SÜSS MicroTec SE exposes the resist for 11 s with the corresponding glass mask in hard contact. The developer AZ® 351B prepares the sample for the coating process which takes place at a base pressure of $2.7 \cdot 10^{-7}$ mbar, a sputtering pressure of $6.4 \cdot 10^{-3}$ mbar, an Argon mass flow of 50 sccm and a power density of 107 W/cm² resulting in a deposition rate for NiCr of 13.3 nm/min. For the final lift-off step, TechniStrip® NI555 is used in an ultrasonic bath for 5 min. Finally, acetone removes remaining resist structures.

With a similar lift-off process, temperature sensors are manufactured. First, an adhesion promotion layer of Titanium with a thickness of 10 nm is applied with a power density of 43 W/cm², 50 sccm Argon and a deposition rate of 20 nm/min. Afterwards, a platinum sputter process with the same power density and argon mass flow results to a platinum deposition rate of 6.6 nm/min and an 84 nm thick actual sensor layer. The base pressure was $2.67 \cdot 10^{-7}$ mbar and the sputtering pressure was $6.1 \cdot 10^{-3}$ mbar. The result is shown in Fig. 3 with the left strain gauges L1 to L3, the middle strain gauges M1 to M4 and the right strain gauges R1 to R6. The layout provides four contact pads for each sensor so that a four-wire technology is possible for each sensor. Thereby, the resistance of supply lines and contact points does not have any impact on the measurement signal.

An annealing step at 250 °C for 1 h under vacuum conditions at a pressure of $8 \cdot 10^{-8}$ mbar completes the process sequence in order to minimize any layer stress and therefore stabilize the initial resistance values of all sensors. Most likely, this annealing is not sufficient to minimize residual stresses that may have been created by grinding and polishing. For contacting, eight circuit boards are attached by using silicone to the substrate in a distance of at least 15 mm to the sensor contact pads to ensure enough

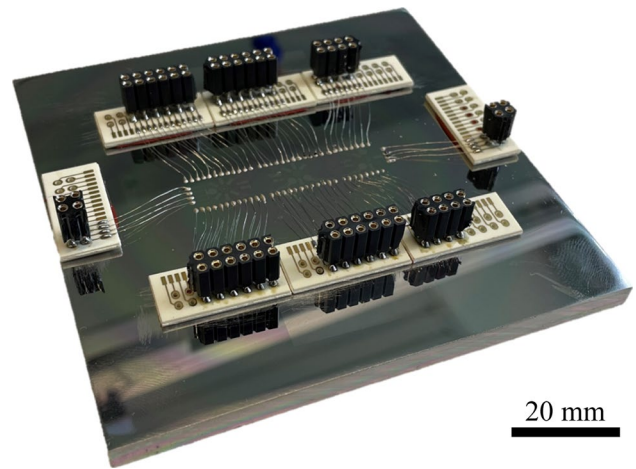


Fig. 4 Stainless steel specimen with directly deposited strain gauges and contacting

space for the drilling device. The electrical conductive two-component silver epoxy adhesive CW2400 from Chemtronics connects the contact pads with thin copper wires that are then soldered to the circuit board. A female connector strip completes the contacting of the sample as shown in Fig. 4.

Now, cables with a pin strip lead the electric signals to a QuantumX MX1615B universal measuring amplifier module from Hottinger Baldwin Messtechnik GmbH which is used for the following temperature and strain measurements. Finally, an adhesive with a thickness of 1 mm is applied only on top of the sensor structures and cured with UV light to embed the sensors. By this, metal chips produced during drilling cannot influence the sensor signals. On the three drilling positions, no adhesive is applied so that the adhesive cannot produce an error concerning the determination of the zero depth position.

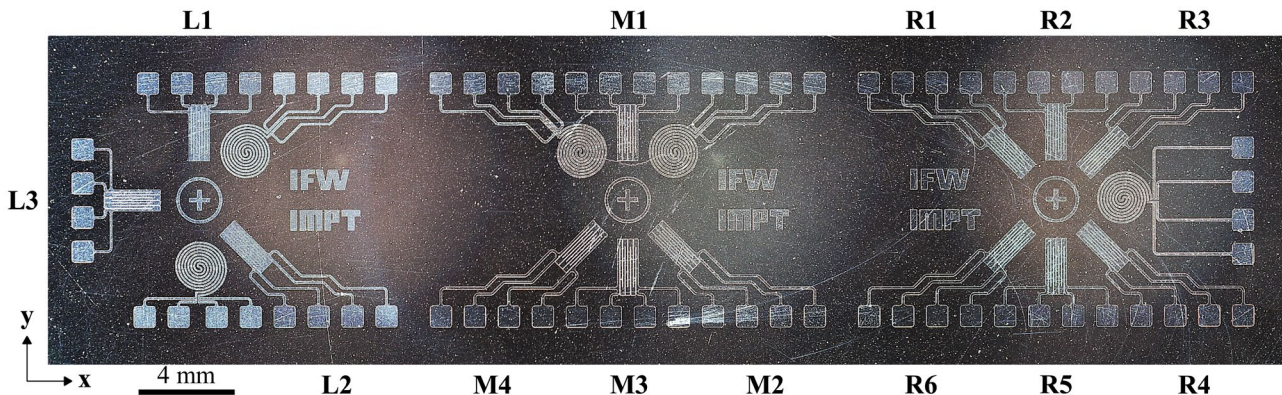


Fig. 3 Directly deposited strain gauges and temperature sensors with an insulation layer on stainless steel. The strain gauges are named according to their belonging to the sensor layout L, M or R (L=Left, M=Middle, R=Right)



Sensor Characterization

Insulation Layer Resistance

First of all, the insulation resistance is measured with a tera-ohm-meter TO3 from Fischer Elektronik. With a measurement voltage of 10 V, a mean value of $5.0 \cdot 10^{12} \pm 1.0 \cdot 10^{12} \Omega$ results which leads to a resistivity of $1.2 \cdot 10^{14} \pm 2.4 \cdot 10^{13} \Omega\text{cm}$. This value indicates a good agreement with the literature [29, 39].

Sensor Layer Resistance

The resistivity of NiCr is $8.5 \cdot 10^{-4} \Omega\text{cm}$ which has been determined before the actual sensor manufacturing. The strain gauges (SG) with an alignment in x- or y-direction (for example L1 or L3) show a resulting mean resistance value of $1505 \pm 27 \Omega$. For the strain gauges with the 45° -alignment (for example L2), the mean value is $1193 \pm 68 \Omega$, as shown in Fig. 5.

For the temperature sensors (TS), a similar behaviour was found. The mean value of the sensors with the alignment in x- or y-direction is $1063 \pm 11 \Omega$, those with the 45° -alignment show a value of $1035 \pm 6 \Omega$. Measurements of the structure width of the glass masks for photolithography do not reveal significant deviations that could explain this behaviour. It is most likely that the substrate surface orientation has an impact which would explain why the impact is much lower for the almost symmetrical layout of the temperature sensors. As it is discussed in “[Temperature coefficient of resistance](#)” section, an anisotropic temperature behaviour of the substrate is expected. During the sputter deposition, a temperature increase is always present. So the reason for the different resistance values could be a different thermal expansion in different directions which would lead to various coating conditions for the strain gauges with different alignments. Due to the fact, that all strain gauges are used in quarter bridge configuration, the resistance value deviations do not affect the following experiments.

Temperature coefficient of resistance

An important parameter for directly deposited strain gauges is the temperature coefficient of resistance (TCR) which indicates the resistance change due to temperature according to equation (1). The lower the TCR, the lower is the temperature impact on the sensor signal resulting in lower measurement errors.

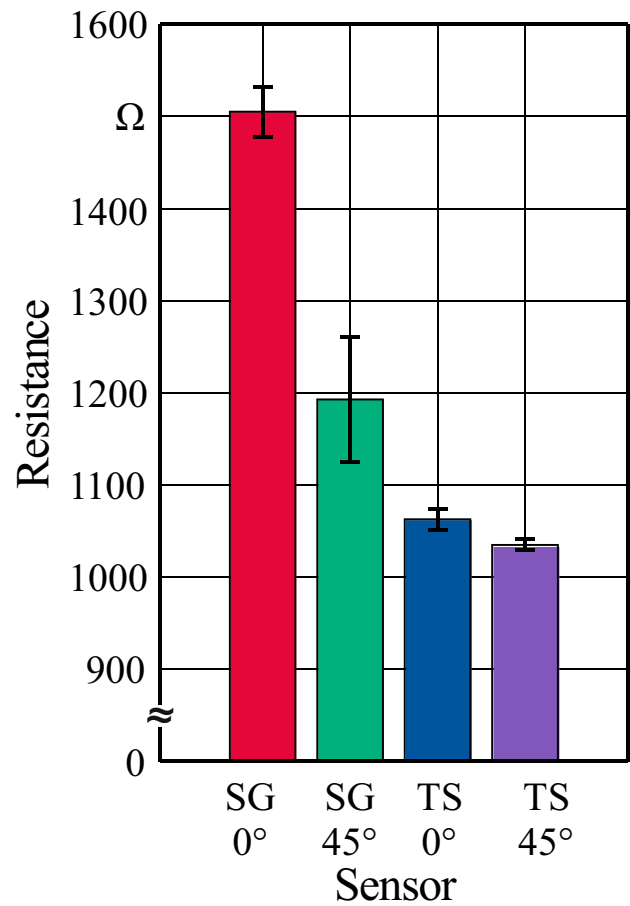


Fig. 5 Mean resistance values for sensors with different alignments. An alignment of 0° means x- or y-direction

$$\text{TCR} = \left[\frac{R_{\text{HT}} - R_{\text{LT}}}{R_{\text{LT}}} \right] / [\text{HT} - \text{LT}] \quad (1)$$

Here, the initial resistance R_{LT} and the resistance R_{HT} describe the measured resistance values at the lowest temperature ($\text{LT} = 20^\circ\text{C}$) and at the highest applied temperature ($\text{HT} = 100^\circ\text{C}$). The tests were carried out on a heating plate. The resistance values show a linear behaviour with increasing temperature (Fig. 6).

The results show negative TCR values close to zero for the NiCr strain gauges and high positive TCR values for the Pt temperature sensors. That is the reason why the curves in Fig. 6 show decreasing (NiCr) and increasing (Pt) behaviour with increasing temperature. A summary of these values is shown in Fig. 7. As a remarkable fact, the results show significant differences between the strain gauges of different angles. Further investigations have to be made to explain this behaviour.

The TCR mean value for strain gauges in x- or y-direction is $-4.1 \pm 1.9 \text{ ppm}/^\circ\text{C}$, whereas the measurements of the strain gauges in 45° -alignment produce a mean value of $-13.2 \pm 5.7 \text{ ppm}/^\circ\text{C}$.



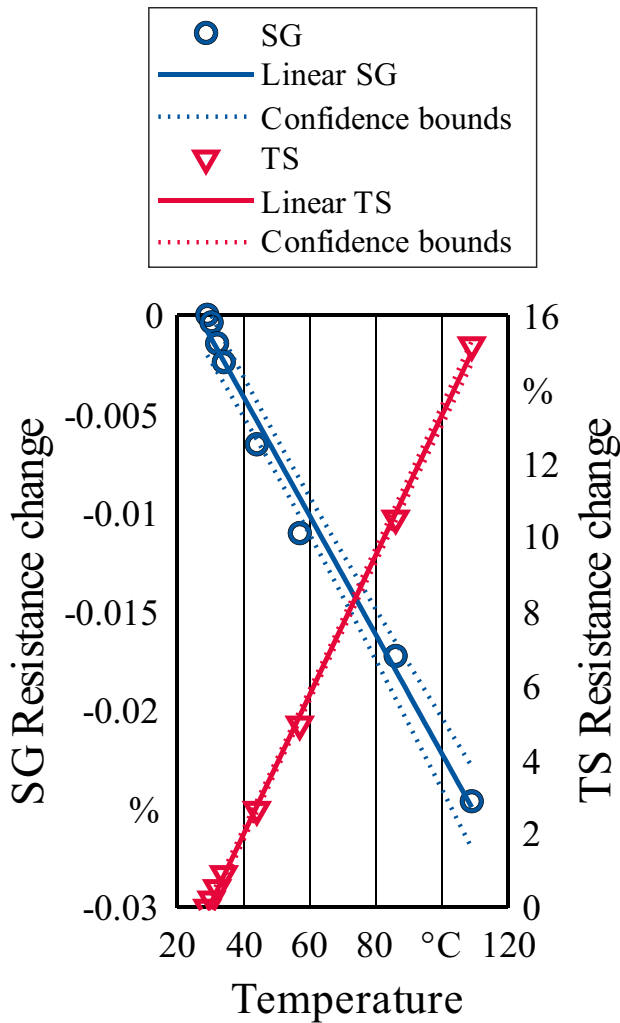


Fig. 6 Exemplary resistance change for a NiCr strain gauge and a Pt temperature sensor with increasing temperature

The TCR mean value of the platinum temperature sensors was calculated to 1937 ± 58 ppm/°C. In this case, no significant variation between differently aligned temperature sensors was detected.

Characterization of the K-Factor

Afterwards, the characterization concerning the k-factor took place in a tensile test stand MultiTest 2.5-xt from Mecmesin. It alternately applies forces of 100 N as a preload (F_{pre}) and 2,000 N as a maximum load (F_{max}) for 20 s each with a constant ramp of 13.3 N/s. This leads to strain values that can be calculated with equation (2).

$$\epsilon = F / (E \cdot A) \tag{2}$$

The remaining values are the Young’s modulus which is $E = 200$ GPa for AISI 304 stainless steel, and the cross

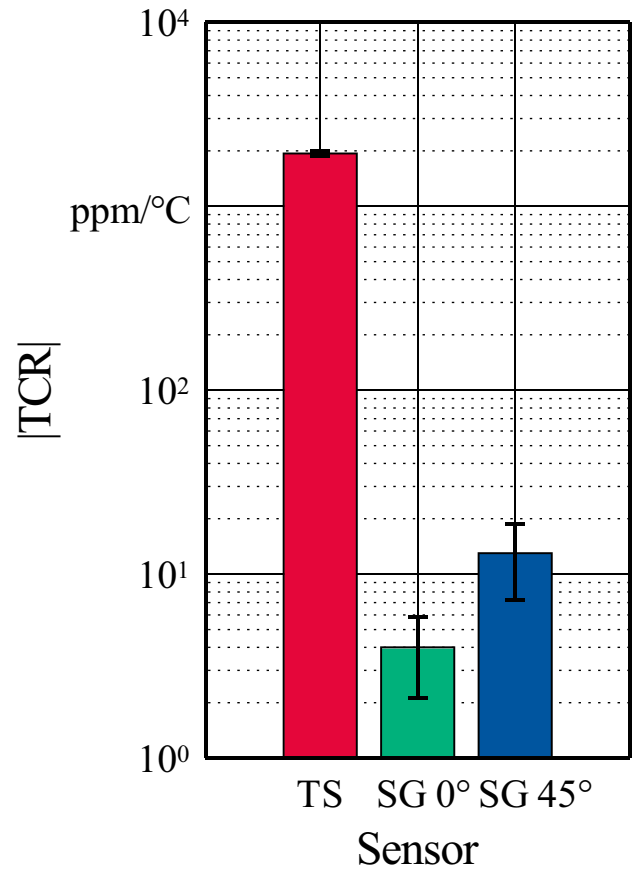


Fig. 7 Mean values for the temperature coefficient of resistance (TCR) for sensors with different alignments. An alignment of 0° means x- or y-direction

sectional area which is $A = 600$ mm² for the sample investigated. The force values result in strain values of $\epsilon_{max} = 16.7$ μm/m and $\epsilon_{pre} = 0.8$ μm/m, whereby the latter is mainly necessary to prevent a sliding of the sample in the clamps that would always occur when load is applied for the first time. With these values and the permanently measured resistance values, the k-factor can finally be calculated as equation (3) shows.

$$k = [(R_{max} - R_{pre}) / R_{pre}] / [\epsilon_{max} - \epsilon_{pre}] \tag{3}$$

For the determination of the k-factor, the strain gauges in y-direction (which corresponds to the strain direction) are chosen. A mean value of $k = 3.0 \pm 0.4$ is measured. For the platinum temperature sensors, the characterization results in a mean value of 1.0 ± 0.5 for their k-factor. This shows that the spiral geometry reduced the effective k-factor which would normally be higher (3.85 according to literature [40] or 3.2 according to own measurements with meander temperature sensors).



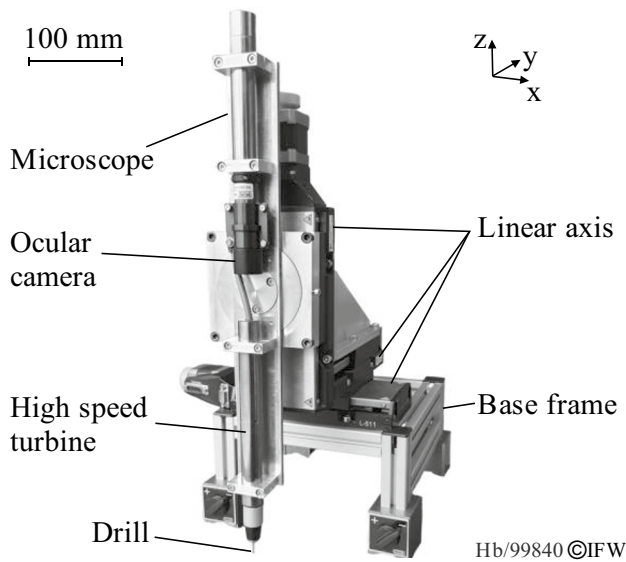


Fig. 8 Bespoke hole drilling device

Incremental Hole Drilling Using Novel and Common Strain Gauge Rosettes

The hole drilling itself was conducted using a bespoke hole drilling device (Fig. 8).

It consists of switchable magnetic feet, a profile frame and three independently controllable linear axes. The z-axis is equipped with a rotatable lock-in mount for a microscope and a high speed turbine. Microscope and turbine ($n_{\max} = 400,000$ rpm) originate from the RS-200 milling guide by Vishay Precision Group, Inc. For accurate positioning of the drill bit by linear axes, the microscope was upgraded with a digital ocular camera. In the investigations presented, common six-blade inverted cone drill bits by Komet Gebr. Brasseler GmbH & Co. KG with a diameter of $d_d = 1.6$ mm were used. Zero point detection was realised by a bespoke electric contact switch. The thickness of the deposited insulation layer of approx. $2 \mu\text{m}$ was ignored for zero point detection. Drilling was performed in conventional plunging mode. For each sensor layout, a new drill was used. The steps were realized automatically and equidistantly ($\Delta z = 0.05$ mm) using a feed speed of $v_z = 0.05$ mm/s up to a depth of $z = 1$ mm. After each drilling step, the drill bit was lifted and held for $t_w = 18$ s to acquire the relaxed strains. Afterwards, the calculation of residual stress depth profiles for common and novel strain gauge rosettes was performed according to ASTM E 837 [6]. Calibration coefficients were corrected for hole diameter. Tikhonov regularization in connection with the Morozov criterion was used. The reference measurements were conducted with commercially available CEA-06-062UL-120 strain gauge rosettes by Vishay Precision Group Inc [34].

Results

In this section, the results for incremental hole drilling with novel and common strain gauges are presented and compared. First strain measurements with novel sensors are shown. Then the evaluation of residual stress depth profiles for novel strain gauge rosettes are discussed. Finally, the residual stress depth profiles obtained from strain measurements with the novel rosettes are compared with reference measurements using common strain gauge rosettes.

Strain Measurements

The strain values show the typical courses that would be expected for incremental hole drilling with common strain gauge rosettes. For most of the novel rosettes investigated, the strain measurements follow smooth trends for the incremental drilling steps (Fig. 9). Exceptions can be seen for strain gauge R5, where measured strains show discontinuous leaps between drilling steps. Reason for this might be a faulty connection of strain gauge and surface of the specimen due to defects in the insulation layer. Here, the insulation resistance shows reduced values in the range of $10 \text{ k}\Omega$ after the measurements. Nevertheless, the strain measurements of the other single gauges can be characterized as suitable for evaluation.

Residual Stress Depth Profiles from Different Sensor Layouts

For evaluation of residual stress depth profiles according to ASTM E 837 standard, different arrangement possibilities for types of standard rosettes result from the sensor layouts (Table 2, Fig. 2).

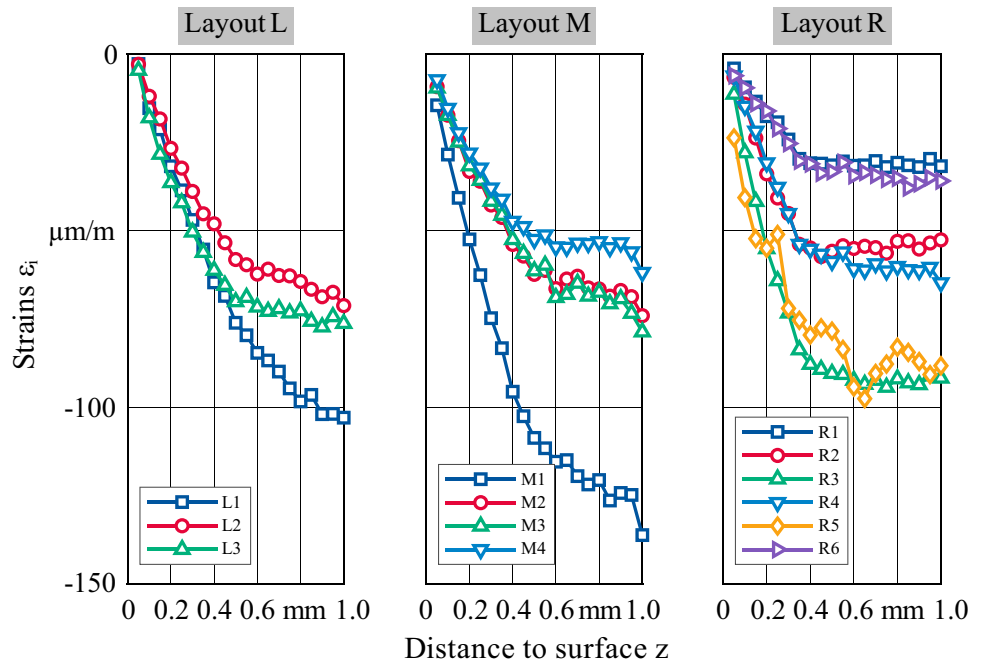
Due to the discontinuous course of strains measured from strain gauge R5, calculated residual stress depths profiles also show discontinuities. Because of different alignments of x-axes for types and arrangements and for better comparability, obtained residual stress depth profiles are presented in principal stresses (σ_{\max} and σ_{\min}).

Comparison of Same Types for Different Layouts

As it can be seen in Fig. 10, the principal residual stress depth profiles show a similar profile for type A arrangements. Maximum and minimum principal stress start at a surface near ($z = 0.05$ mm) tensile residual stress state of about $\sigma_{\max} = 200$ MPa or $\sigma_{\min} = 150$ MPa. This tensile stress state decreases and reaches a 0-near level at $z = 0.6$ mm. Only the stress state of sensor layout M increases again to a tensile state of about $\sigma_{\max} = 150$ MPa or $\sigma_{\min} = 90$ MPa



Fig. 9 Strain measurements of single thin film strain gauges in the different sensor layouts L, M and R



in a depth of $z > 0.8$ mm. The profile of the second Type A arrangement of sensor layout R is comparably discontinuous and shows a higher and implausible (approx. 550 MPa) surface near tensile stress state. This can be explained by the discontinuous measured strains of strain gauge R5 in combination with the numerical instability of the integral method. Nevertheless it can be stated that the sensor layouts of type A arrangements show similar results.

The same observations can be made for residual stress depth profile calculations of the arrangements of Type B (Fig. 11). The course of the profiles is similar to the ones shown in Fig. 10. Both of the figures generally show the feasibility of novel strain gauges for use with the hole drilling method.

Comparison of Different Types for Same Layouts

The general feasibility allows for a comparison of the repeatability of the hole drilling method due to the usage

Table 2 Sensor layouts and possible arrangements

Layout	Type	Arrangement for $\epsilon_1-\epsilon_2-\epsilon_3$
L	A	L3-L2-L1
M	A	M2-M1-M4
	B	M2-M3-M4
R	A	R1-R5-R3
		R4-R2-R6
	B	R1-R2-R3
		R4-R5-R6

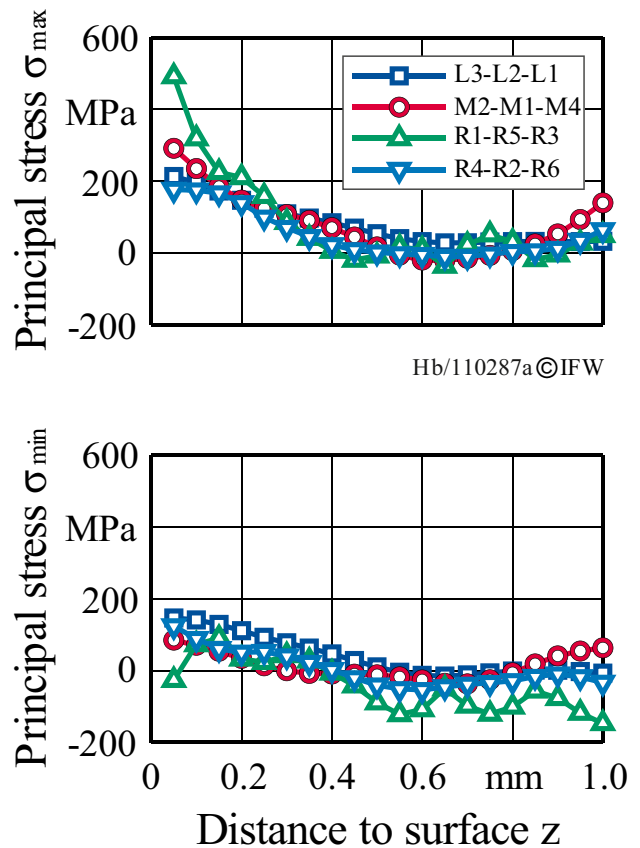


Fig. 10 Calculated principal residual stress depth profiles for arrangements of Type A



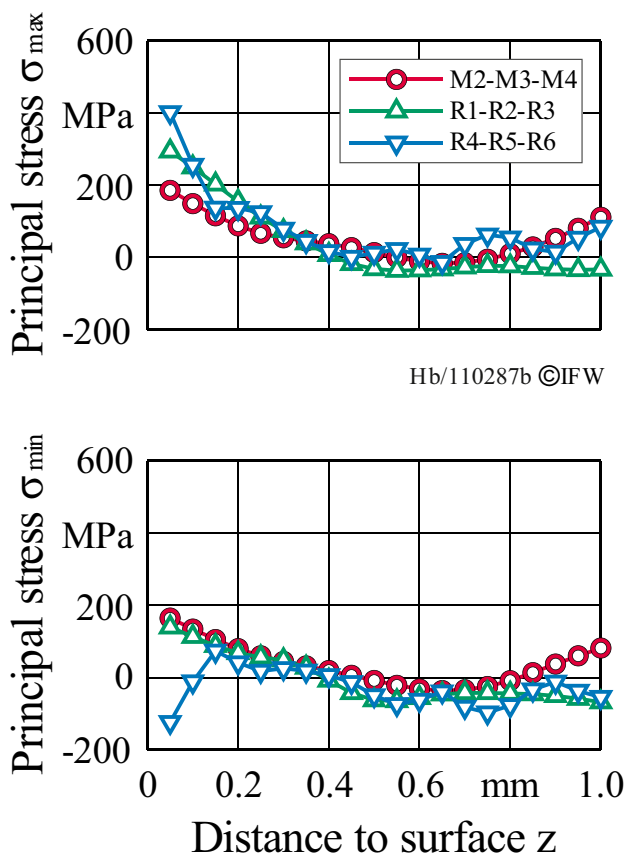


Fig. 11 Calculated principal residual stress depth profiles for arrangements of Type B

of different types for the same layouts. Common hole drilling strain gauge rosettes mostly contain three single strain gauges. By using more than three strain gauges, more information about the strain state around the induced hole can be derived. This leads to the possibility of calculating mean values and standard deviations along the depth profiles by evaluation of different arrangements on sensor layouts M and R.

For layout M, the different arrangements show slightly different values down to a depth of $z < 0.5$ mm (Fig. 12). In further depths, the calculated principal residual stresses are nearly identical. These deviations probably result from specimen geometry, relative position of the axis of the high speed turbine to the specimen or hole eccentricity. The axis of the turbine might be inclined and not ideally perpendicular to the surface of the specimen. This results in unequally removed material, causing first strain releases that are detected more pronounced on single gauges than on others.

The same effects can be seen for sensor layout R (Fig. 13), although the differences of residual stress values between the different arrangements are smaller compared to sensor layout M (Fig. 12). Due to the discontinuous course of measured strains of strain gauge R5, the derived residual stress depth

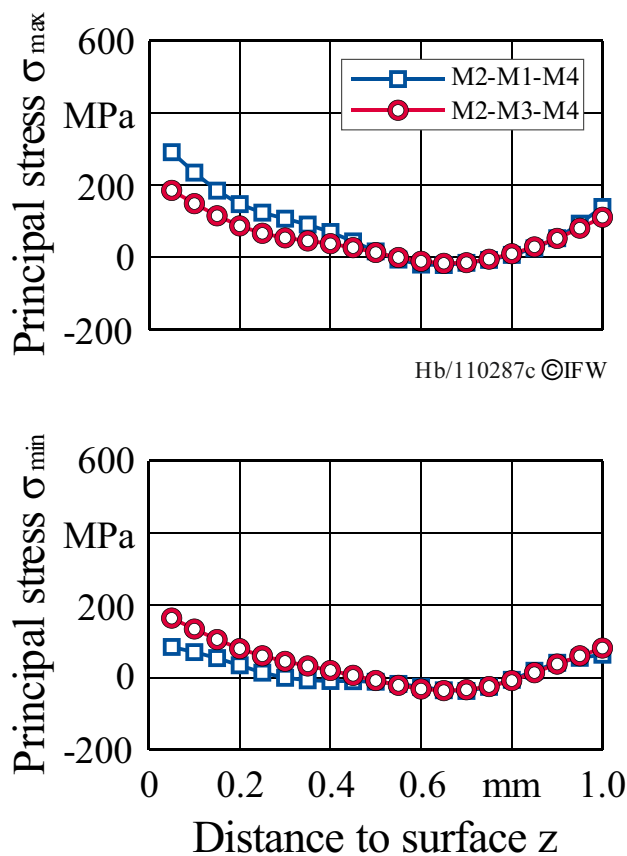


Fig. 12 Calculated residual stress depth profiles for Type A and B arrangement of sensor layout M

profiles calculated from strains of strain gauge R5 show similar courses and minor differences in values.

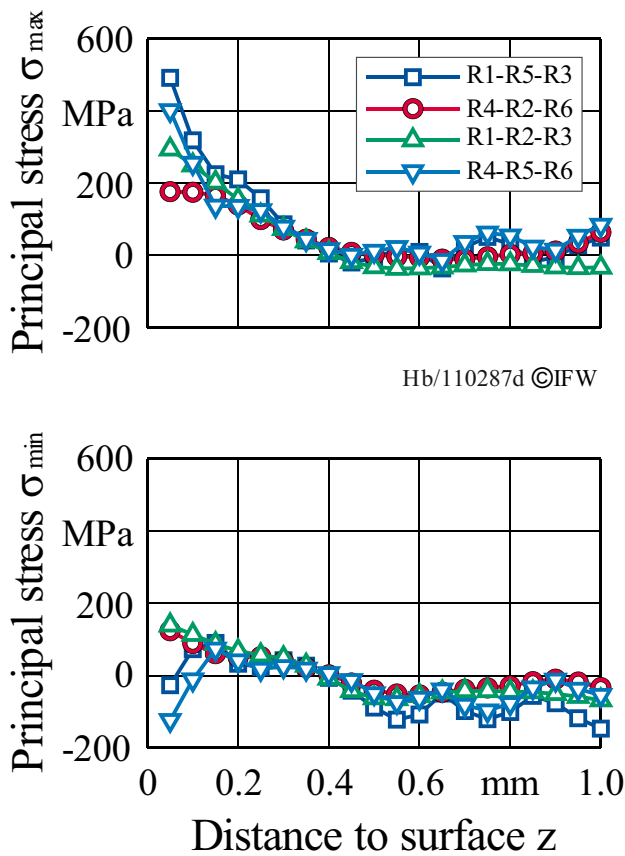
Comparison of Novel Sensors with Conventional Sensors

For validation of the residual stress depth profiles derived from directly deposited sensors, two reference measurements with CEA-06-062UL-120 strain gauges from Vishay Precision Group Inc. on the same specimen with same surface preparation have been conducted. The measurement positions were ± 15 mm in y-direction from measurement position of sensor layout M.

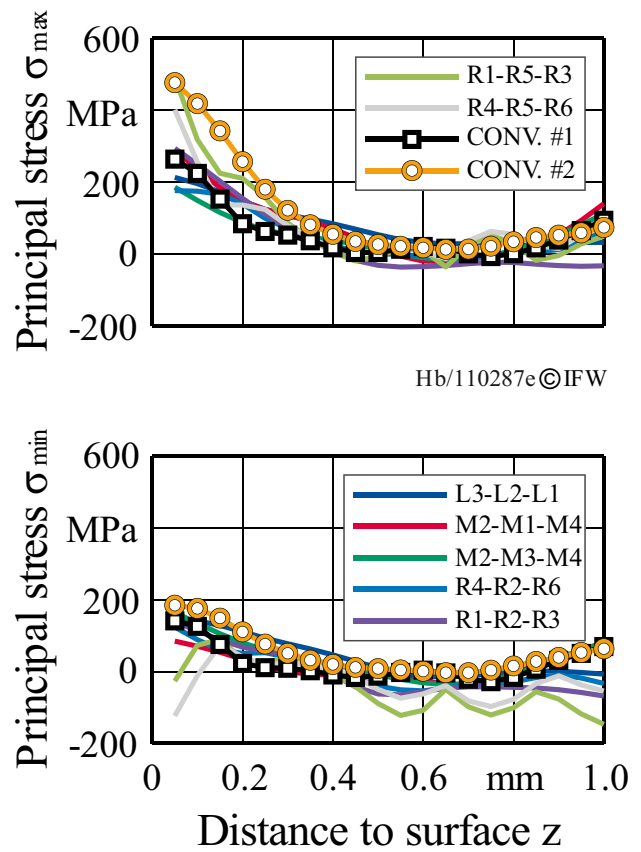
Therefore, any of the calculated profiles derived from novel sensors (Type A and B) are directly compared with the profiles derived from conventional sensors (Fig. 14).

It can be seen that the courses of conventional sensors are quite similar to the ones obtained from novel sensors. The first measurement with the conventional sensor (CONV. #1) shows relatively high, implausible surface near tensile residual stress values. They start from $\sigma_{\max} = 480$ MPa decreasing to below 200 MPa at $z = 0.25$ mm. The high surface near residual stress state might indicate that the depth profiles obtained from novel sensors with layouts containing strain measurements from





Hb/110287d ©IFW



Hb/110287e ©IFW

Fig. 13 Calculated residual stress depth profiles for Type A and B arrangement of sensor layout R

Fig. 14 Comparison of residual stress depth profiles for novel and conventional strain gauge rosettes

strain gauge R5 are plausible. Nevertheless, after $z=0.25$ mm the stress values approximate the course of residual stress values from the measurement with the conventional sensor CONV. #2 and the general course of depth profiles obtained from measurements with the novel sensors.

Considering Fig. 14, there is a high coincidence of residual stress depth profiles obtained from conventional and novel sensors. Profiles obtained from strain measurements with sensor R5 still deviate, as mentioned above.

Temperature measurements are not presented due to the fact that during drilling a maximum increase of $\Delta T=2$ °C was measured. Thus, measurement errors resulting from temperature increase were neglected.

Summary and Outlook

The general feasibility of directly deposited thin-film strain gauges for the incremental hole drilling method is presented. Therefore, different arrangements (Type A, B) for novel sensors regarding principal residual stresses have been evaluated. The evaluations of different arrangements within the novel sensors show consistent residual stress depth profiles

which have been validated by measurements with conventional sensors.

As shown in the investigations, the novel sensors can also be prone to errors. Due to an insufficient insulation from a single strain gauge to the substrate, discontinuous strain depth profiles and thus discontinuous and partly implausible residual stress depth profiles are obtained (see strains of R5 in Fig. 8). Here, the cleaning after polishing, the plasma pre-treatment and the development of an insulation layer with an even higher yield could prevent this error.

Residual stress depth profiles of novel and conventional sensors generally do not show complete coincidence. It is a possibility that this might be because the measurement positions of novel and conventional sensors were different. Thus, local differences or variations in residual state from sheet manufacturing and specimen preparation (grinding, polishing) would be inherent.

Although there are several uncertainties regarding calibration coefficients and strain measurement that can be minimized by using directly deposited strain gauges, further uncertainties remain that have not been considered in this study. These are e. g. variations in material properties of the specimen or resulting hole geometry and



eccentricity, leading to deviations in calculated residual stress depth profiles.

From the investigations presented, the following conclusions can be drawn:

- (1) The novel directly deposited strain gauges are feasible for incremental hole drilling.
- (2) Using the direct deposition process, any desired rosette geometry can be applied resulting in a free derivation of strain fields around the induced hole.
- (3) The comparison of novel sensors with conventional sensors has been shown for residual stress depth profiles. Detailed investigations on the improvement of the single uncertainty sources are still necessary.

In further investigations, the directly deposited sensors in combination with the hole drilling method will be tested on stress relieved specimens that are applied with calibration loads from a tensile testing machine. Inverse calculations will compare theoretically expected strains with the strains obtained from hole drilling measurements.

Additional Finite Element simulations will be conducted to quantify the improvement of directly deposited sensors regarding calibration coefficients (influence of adhesive and zero depth setting). The simulations will also be used to prove the possibility for usage with thermally sprayed thick film systems and whether adjustments to common calibration coefficients are necessary.

Afterwards, the directly-deposited sensors will be used in thermally sprayed thick film systems as mentioned in the introduction. Therefore, a novel, unique coating system will be used, which has been developed especially for this application. This novel coating system will have the possibility to protect the sensors from thermomechanical stressing during the spraying process. With these sensors new information on the residual stress state of thermally sprayed thick film systems will be gained.

These directly deposited sensors will be one research area of the new Leibniz Universität Hannover based research building ‘SCALE – Tomorrow’s Scalable Production Systems’.

Supplementary Information The online version contains supplementary material available at <https://doi.org/10.1007/s11340-022-00822-0>.

Acknowledgements The authors thank the German Federation of Industrial Research Associations (AiF) for the financial support of the project “Deep rolled welds – Increased fatigue strength of welded joints in wind energy by deep rolling”, grant number 20626/N.

Funding Open Access funding enabled and organized by Projekt DEAL.

Declarations

Conflict of Interest The authors declare that they have no conflict of interest.

Open Access This article is licensed under a Creative Commons Attribution 4.0 International License, which permits use, sharing, adaptation, distribution and reproduction in any medium or format, as long as you give appropriate credit to the original author(s) and the source, provide a link to the Creative Commons licence, and indicate if changes were made. The images or other third party material in this article are included in the article’s Creative Commons licence, unless indicated otherwise in a credit line to the material. If material is not included in the article’s Creative Commons licence and your intended use is not permitted by statutory regulation or exceeds the permitted use, you will need to obtain permission directly from the copyright holder. To view a copy of this licence, visit <http://creativecommons.org/licenses/by/4.0/>.

References

1. Klaas D, Ottermann R, Dencker F, Wurz MC (2020) Development Characterisation and High-Temperature Suitability of Thin-Film Strain Gauges Directly Deposited with a New Sputter Coating System. *Sensors* 20:3294. <https://doi.org/10.3390/s20113294>
2. Valente T, Bartuli C, Sebastiani M, Loreto A (2005) Implementation and Development of the Incremental Hole Drilling Method for the Measurement of Residual Stress in Thermal Spray Coatings. *J Therm Spray Technol* 14:462–470. <https://doi.org/10.1361/105996305X76432>
3. Obelode E, Gibmeier J (2013) Influence of the Interfacial Roughness on Residual Stress Analysis of Thick Film Systems by Incremental Hole Drilling. *MSF* 768–769:136–143. <https://doi.org/10.4028/www.scientific.net/MSF.768-769.136>
4. Held E, Gibmeier J (2015) Application of the Incremental Hole-Drilling Method on Thick Film Systems—An Approximate Evaluation Approach. *Exp Mech* 55:499–507. <https://doi.org/10.1007/s11340-014-9962-3>
5. Rendler NJ, Vigness I (1966) Hole-drilling strain-gage method of measuring residual stresses. *Exp Mech* 6:577–586. <https://doi.org/10.1007/BF02326825>
6. ASTM International (2020) ASTM E837: Test Method for Determining Residual Stresses by the Hole-Drilling Strain-Gage Method. ASTM, Pennsylvania
7. Schajer GS (1988) Measurement of Non-Uniform Residual Stresses Using the Hole-Drilling Method Part II—Practical Application of the Integral Method. *J Eng Mater Technol* 110:344–349. <https://doi.org/10.1115/1.3226060>
8. Schajer GS (1988) Measurement of Non-Uniform Residual Stresses Using the Hole-Drilling Method Part I—Stress Calculation Procedures. *J Eng Mater Technol* 110:338–343. <https://doi.org/10.1115/1.3226059>
9. Blödorn R, Bonomo LA, Viotti MR, Schroeter RB, Albertazzi A (2017) Calibration Coefficients Determination Through Fem Simulations for the Hole-Drilling Method Considering the Real Hole Geometry. *Exp Tech* 41:37–44. <https://doi.org/10.1007/s40799-016-0152-3>
10. Nau A, Scholtes B (2013) Evaluation of the High-Speed Drilling Technique for the Incremental Hole-Drilling Method. *Exp Mech* 53:531–542. <https://doi.org/10.1007/s11340-012-9641-1>
11. Nau A, von Mirbach D, Scholtes B (2013) Improved Calibration Coefficients for the Hole-Drilling Method Considering the



- Influence of the Poisson Ratio. *Exp Mech* 53:1371–1381. <https://doi.org/10.1007/s11340-013-9740-7>
12. Sobolevski EG, Scholtes B (2010) Eigenspannungsanalysen nach der Bohrlochmethode unter Verwendung geometriespezifischer Kalibrierfunktionen. *Mater Test* 52:356–362. <https://doi.org/10.3139/120.110136>
 13. Schajer GS, Altus E (1996) Stress Calculation Error Analysis for Incremental Hole-Drilling Residual Stress Measurements. *J Eng Mater Technol* 118:120–126. <https://doi.org/10.1115/1.2805924>
 14. Scafidi M, Valentini E, Zuccarello B (2011) Error and Uncertainty Analysis of the Residual Stresses Computed by Using the Hole Drilling Method. *Strain* 47:301–312. <https://doi.org/10.1111/j.1475-1305.2009.00688.x>
 15. Peral D, de Vicente J, Porro JA, Ocaña JL (2017) Uncertainty analysis for non-uniform residual stresses determined by the hole drilling strain gauge method. *Measurement* 97:51–63. <https://doi.org/10.1016/j.measurement.2016.11.010>
 16. Oettel R (2000) Manual of Codes of Practice for the Determination of Uncertainties in Mechanical Tests on Metallic Materials: Code of Practice No. 15: The Determination of Uncertainties in Residual Stress Measurement (Using the hole drilling technique). UNCERT COP 1:1–18
 17. Nau A (2015) A contribution to enlarge the application limits of residual stress analyses by the hole-drilling and the ring-core method Dr.-Ing Thesis. Universität Kassel, Kassel. ISBN 978-3-737-60054-5
 18. Hottinger Baldwin Messtechnik GmbH (2021) Strain Gauges: First choice for strain measurements. Darmstadt. Available online: <https://www.hbm.com/fileadmin/mediapool/hbmdoc/technical/S01265.pdf>, last checked 18.06.2021
 19. VDI – The Association of German Engineers (2015) VDI 2635 Sheet 1: Experimental structure analysis - Metallic bonded resistance strain gauges - Characteristics and testing conditions. ICS no. 17.040.30
 20. VDI – The Association of German Engineers (2019) 2635 Sheet 2: Experimental structure analysis - Recommendation on the implementation of strain measurements at high temperatures. ICS no. 17.040.30
 21. Keil S (2017) *Dehnungsmessstreifen*, Springer Fachmedien Wiesbaden. ISBN 978-3-658-13611-6
 22. Yang S, Zhang C, Wang H, Ding G (2017) An in-situ prepared synchronous self-compensated film strain gage for high temperature. In: IEEE 30th International Conference, p 1021–1024. <https://doi.org/10.1109/MEMSYS.2017.7863585>
 23. Heckmann U, Bandorf R, Gerdes H, Lübke M, Schnabel S, Bräuer G (2009) New materials for sputtered strain gauges. *Proc Chem* 1:64–67. <https://doi.org/10.1016/j.proche.2009.07.016>
 24. Hoffmann K (2016) An Introduction to Stress Analysis using Strain Gauges. Hottinger Baldwin Messtechnik GmbH, Darmstadt
 25. Bandorf R, Gerdes H, Heckmann U, Bräuer G, Petersen M (2012) Hochempfindliche Dünnschicht-Dehnungsmessstreifen auf technischen Bauteilen: High-sensitive thin-film strain gauges on technical components, 16. GMA/ITG-Fachtagung Sensoren und Messsysteme 423–434. <https://doi.org/10.5162/sensoren2012/4.1.3>
 26. Klaas D, Becker J, Wurz MC, Schlosser J, Kunze M (2016) New coating system for direct-deposition of sensors on components of arbitrary size: A novel approach allowing for thinner sensors with higher measuring accuracy. *IEEE Sensors* 1–3. <https://doi.org/10.1109/ICSENS.2016.7808440>
 27. Klaas D, Wurz MC (2017) Direct Deposition of Sensors on Technical Surfaces. In: Denkena B, Morke T (eds) *Cyber-physical and gentelligent systems in manufacturing and life cycle*. Elsevier Science Publishing Co, Amsterdam, pp 187–209
 28. Bach W, Becker J, Rissing L, Wurz MC (2014) Beschichtungseinrichtung zum zumindest teilweisen Beschichten einer Oberfläche. Patent DE102014004323A1
 29. Ottermann R, Klaas D, Dencker F, Wurz MC, Hoheisel D, Rottengatter P, Kruspe T (2020) Direct Deposition of Thin-Film Strain Gauges with a New Coating System for Elevated Temperatures. *IEEE Sensors* 1–4. <https://doi.org/10.1109/SENSORS47125.2020.9278661>
 30. Dencker F, Schlenkrich A, Wurz MC (2017) Press hardening tool integrated thin film temperature sensor. EUSPEN ISBN 9780995775107, Proceedings of the 17th International Conference of the European Society for Precision Engineering and Nanotechnology (EUSPEN)
 31. Arndt M, Dencker F, Wurz MC (2019) Novel Eddy-Current Sensor for Industrial Deep-Drawing Applications. *IEEE*, Montreal QC Canada, pp 1–4. <https://doi.org/10.1109/SENSORS43011.2019.8956948>
 32. Dencker F, Wurz M, Dubrovskiy S, Koroleva E (2016) An application report: Protective thin film layers for high temperature sensor technology. In: IEEE NW Russia Young Researchers in Electrical and Electronic Engineering Conference (EIConRusNW), St. Petersburg. IEEE, pp 32–36. <https://doi.org/10.1109/EIConRusNW.2016.7448110>
 33. Ottermann R, Klaas D, Dencker F, Hoheisel D, Jung S, Wienke A, Düsing JF, Koch J, Wurz MC (2021) Directly Deposited Thin-Film Strain Gauges on Curved Metallic Surfaces (in review process). *IEEE Sensors* 1–4
 34. Vishay Precision Group (2010) Tech-Note TN-503: Measurement of Residual Stresses by the Hole-Drilling Strain Gage Method
 35. Deutsche Edelstahlwerke () Data sheet 1.4301 Chromium-nickel austenitic stainless steel, 01.08.07. https://www.dew-stahl.com/fileadmin/files/dew-stahl.com/documents/Publikationen/Werkstoffdatenblaetter/RSH/1.4301_de.pdf. Accessed 18 Jun 2021
 36. Deutsches Institut für Normung (2013) DIN EN ISO 16610-21 Geometrische Produktspezifikation (GPS) - Filterung - Teil 21: Lineare Profilfilter: Gauß-Filter, ICS 17.040.40
 37. Prevey PS (1988) Residual-stress distributions produced by strain-gage surface preparation. *Exp Mech* 28:92–97. <https://doi.org/10.1007/BF02329002>
 38. International Syalons () Data sheet Alumina. <https://www.syalons.com/wp-content/uploads/2018/03/aluminon-999-datasheet.pdf>. Accessed 18 Jun 2021
 39. Bartzsch H, Glöß D, Frach P, Gittner M, Schultheiß E, Brode W, Hartung J (2009) Electrical insulation properties of sputter-deposited SiO₂ Si₃N₄ and Al₂O₃ films at room temperature and 400 °C. *Phys Status Solidi A* 206:514–519. <https://doi.org/10.1002/pssa.200880481>
 40. Fricke S, Friedberger A, Mueller G, Seidel H, Schmid U (2008) Strain gauge factor and TCR of sputter deposited Pt thin films up to 850°C. *IEEE Sensors* 1532–1535. <https://doi.org/10.1109/ICSENS.2008.4716739>

